Thin Solid Films 647 (2018) 33–39

Contents lists available at ScienceDirect

Thin Solid Films

journal homepage: www.elsevier.com/locate/tsf

Study on the photochemical preparation of nickel gallium oxide spinel doped with Eu(III) ions from carboxylate and β-diketonate complexes and the evaluation of its optical properties

G. Cabello-Guzman[a,*], L. Lillo-Arroyo[a], C. Caro-Díaz[a], F. Valenzuela-Melgarejo[a], A. Fernandez-Perez[b], G.E. Buono-Core[c], B. Chornik[d]

[a] Departamento de Ciencias Básicas, Facultad de Ciencias, Universidad del Bío-Bío, Chillán, Chile
[b] Departamento de Física, Facultad de Ciencias, Universidad del Bío-Bío, Concepción, Chile
[c] Instituto de Química, Pontificia Universidad Católica de Valparaíso, Valparaíso, Chile
[d] Deparamento de Física, Facultad de Ciencias Físicas y Matemáticas, Universidad de Chile, Santiago 8370415, Chile

ARTICLE INFO

Keywords:
Photodeposition
Thin films
Optical properties
Photoluminescense

ABSTRACT

In this work, Ni(II) carboxylate and Ga(III) β-diketonate complexes, were studied as precursors for the photochemical deposition of ternary metal oxide thin films with different levels of Eu(III) doping. Diluted solutions of these complexes were mixed, spin-coated on silicon(100) and irradiated at room temperature with a 254 nm UV light. Subsequently, the photodeposited films were annealed at 350, 650 and 950 °C. The photochemistry and annealing of these films was monitored by Fourier transform infrared spectroscopy. The obtained samples were characterized by X-ray diffraction, X-ray photoelectron spectroscopy, scanning electron microscopy and UV–vis spectroscopy. The results showed the formation of spinel-type structures ($NiGa_2O_4$). The prepared phosphors under UV irradiation revealed red luminescence, which was attributed to transitions from the $^5D_0$ excited state to the ^7F_j ground states of the Eu^{3+} ions. The intensity of the photoluminescence decreases upon Eu doping, and the performance of these emissions depends strongly on the surface structure and morphology of the photodeposited films.

1. Introduction

Spinels are a class of mixed metal oxides of chemical composition AB_2O_4, where A is a metal ion with valence (+2) and B is a metal ion with valence (+3). In the spinel structure, the oxygen ions form lattice face centered cubic and the A and B cations occupy the interstitial sites of the tetrahedron and the octahedron, depending on the particular type of spinel [1]. The first studies were focused on the synthesis and characterization of this material. The feasibility of introducing various cations of different charges and sizes into the crystalline structure of the spinel, has given rise to new optical properties [2,3]. For example, the study of spinel materials doped with lanthanide (Ln^{III}) ions has attracted much interest due to their wide spectral range emission, from ultraviolet to infrared [4]. Among all Ln^{III} ions, europium is the most attractive for photoluminescent studies due to its narrow band emission between the 610–625 nm and a long lifetime of its excited states [5]. Usually Europium has two oxidation states and show different types of emission spectrum. The emission signal of Eu(III) is composed of red-colored narrow lines with energies that are, in some cases, independent of the host lattice. On the other hand, the emission spectra of Eu(II) is composed of a broad band with an energy strongly depending on the crystal environment [5]. Thus, the divalent europium ion provides a luminescence in which the color depends on the host lattice, varying from ultraviolet to red. Among these oxide phosphors, gallium compounds, such as $ZnGa_2O_4$ [6] and $MgGa_2O_4$ [7], have been studied as host materials for lanthanide ion-doped phosphors. Some difficulties in the preparation of these mixed-oxide materials include: low purity in the chemical composition, loss of homogeneity in the size and distribution of the particles, and high calcination temperatures. In this context, various methods of synthesis have been proposed for the preparation of mixed-oxide metal materials. Each of these methods of synthesis determines the quality of the material in terms of its morphology, structure and chemical composition. All these factors finally define the properties of material and thus the potential applications.

Photochemical deposition methods differ from other synthetic techniques due to the selectivity of the precursor species for the deposition of the desired material. In this case, the precursor species must be photo-reactive by the absorption of light generating an intermediate

* Corresponding author.
E-mail address: gcabello@ubiobio.cl (G. Cabello-Guzman).

https://doi.org/10.1016/j.tsf.2017.12.017
Received 10 August 2017; Received in revised form 7 December 2017; Accepted 19 December 2017
Available online 20 December 2017

species or the final product of the photochemical reaction [8]. In recent years, we have developed a photochemical method based on the use of UV light for the deposition of some metal oxide thin films in order to study their photoluminescent characteristics [9–11]. In general, the application of this methodology involves a series of steps: (i) choosing suitable coordination complex precursors, (ii) deposition of the solutions of the precursors onto substrates using the spin-coating technique, (iii) irradiation of the spin-coated films with light of a proper wavelength to decompose the complex precursors and to form metal oxide films, under aerated conditions, (iv) elimination of organic residues from the films using organic solvents and (v) post-annealing of the photodeposited films.

In this manuscript, we report a photochemical synthesis as an alternative methodology for the preparation of ternary metal oxide thin films of $NiGa_2O_4$ doped with Eu(III) ions. The effect of europium doping on the luminescent properties of the thin films was also studied.

2. Experimental details

2.1. Preparation of amorphous thin films

The precursor complexes Ni(2-ethylhexanoate)$_2$ and Ga(acac)$_3$ were purchased from Aldrich Chemical Company. The substrates for film deposition were quartz plates (2×2 cm^2) and n- and p-type silicon (100) wafers (1×1 cm^2), which were obtained from Wafer World Inc., Florida, USA.

The Ni(2-ethylhexanoate)$_2$ and Ga(acac)$_3$ complexes were homogenized and mixed in a molar proportion of 1:2 in CH_2Cl_2 or ethanol solution. The thin films were prepared as follows. A silicon chip was placed on a spin-coater and rotated at a speed of 600 rpm. A portion (0.5 ml) of a solution of both precursor complexes in CH_2Cl_2 was deposited onto the silicon chip and allowed to spread. The motor was stopped after 30 s, and a thin film of the complex remained on the chip. The quality of the films was examined using optical microscopy (500 × magnification).

For the deposition of $NiGa_2O_4$:xEu films, solutions of both Ni(2-ethylhexanoate)$_2$ and Ga(acac)$_3$ with different proportions of Eu(acac)$_3$ (where x = 5, 10 and 15 mol%) were spin-coated on the appropriate substrate, and the thin films were irradiated until no absorptions due to the complexes were observed in the infrared spectrum.

2.2. Photolysis of the complexes as films on Si(100) surfaces

All photolysis experiments were performed following identical procedures. First, the Fourier transform infrared spectroscopy (FT-IR) spectrum of the starting film was obtained. Then, the chip was placed under a UV-lamp setup, which was equipped with two 254 nm 6 W tubes in air. The reaction progress was monitored by recording the FT-IR spectrum at different time intervals, following a decrease in the IR absorption of the complexes. After the FT-IR spectrum showed no evidence of the starting material, the chip was rinsed several times with dry acetone to remove all remaining organic products on the surface prior to analysis. To obtain films of a specific thickness, successive layers of the precursor materials were deposited by spin-coating and irradiated as previously described. This process was repeated several times until the desired thickness was achieved. Post-annealing was performed under a continuous flow of synthetic air at different temperatures (350–950 °C) for 2 h in a programmable Lindberg tube furnace.

2.3. Characterization of the thin films

The FT-IR spectra were obtained with 4 cm^{-1} resolution in a Perkin Elmer Spectrum Two FT-IR spectrophotometer. The UV spectra were obtained with 1 nm resolution in a Perkin Elmer Model Lambda 25 UV–vis spectrophotometer. X-ray diffraction (XRD) patterns were obtained using a D8 Advance Bruker X-ray diffractometer; the X-ray source was Cu Kα radiation (40 kV/30 mA). X-ray photoelectron spectroscopy (XPS) were recorded on an XPS-Auger Perkin Elmer electron spectrometer Model PHI 1257, which included an ultra-high vacuum chamber, a hemispherical electron energy analyzer and an X-ray source that provided unfiltered Kα radiation from its Al anode ($h\nu$ = 1486.6 eV). The pressure of the main spectrometer chamber during data acquisition was maintained ca. 10^{-7} Pa. The binding energy (BE) scale was calibrated using the peak of adventitious carbon, which was set to 284.6 eV. The accuracy of the BE scale was ± 0.1 eV. The morphology and existence of elements in the samples were obtained by scanning electron microscopy (SEM) with a Hitachi model SU 3500 with an accelerating voltage of 10.0 kV. The SEM was coupled with a Bruker model Quantax 100 energy dispersive X-ray spectroscope (EDX) for semi-quantitative determinations.

Photoluminescence (PL) emission spectra measurements were carried out in an Ocean Optics Model QE65000-FL spectrometer with an L-type setup. Excitation was performed with a PX-2 pulsed xenon lamp (220–750 nm), and the UV light passed through a monochromator set at 325 nm. The measurements were taken at room temperature.

3. Results and discussion

3.1. Solid-state photoreactivity of the precursor complexes

Some coordination and organometallic complexes, such as Ni(acac)$_2$ [12,13], Ni(t-amyltropolonate)$_2$ [14], Ni(CO)$_2$(PPh$_3$)$_2$ [15], Ga(tmhd)$_3$ [10,11] and Ga(acac)$_3$ [16], have been used as precursors in the photodeposition of metal oxides, such as NiO and Ga_2O_3 thin films. It is known that these complexes absorb strongly at readily accessible parts of the UV spectrum (200–400 nm) and that irradiation of these complexes with UV light leads to the photoreduction and photofragmentation of these complexes. Here, we proposed the use of Ni(2-ethylhexanoate)$_2$ and Ga(acac)$_3$ complexes as precursors for the photodeposition of ternary metal oxides (Eq. (1)).

$$NiL_{2(\text{thin film})} + 2Ga(acac)_{3(\text{thin film})} + xEu(acac)_{3(\text{thin film})} + h\nu + O_2 \rightarrow NiGa_2O_{4-X}\text{: } xEu_{(\text{thin film})} \quad (1)$$

where L = 2-ethylhexanoate, acac = acetylacetonate and x = 5, 10 and 15 mol% of Eu.

To evaluate the solid-state photoreactivity of the mixed precursor complexes, solutions of Ni(2-ethylhexanoate)$_2$ and Ga(acac)$_3$ in a molar proportion of 1:2, respectively, were deposited on Si wafers by spin-coating and irradiated in air with a 254 nm UV source. The FT-IR spectral changes associated with the photoreactivity of both precursor complexes after different irradiation times are depicted in Fig. 1. The photolysis of these complexes resulted in the gradual loss of intensity associated with the vibrational modes at 2950 cm^{-1} associated to a single carbon-hydrogen bond (C—H); at 1590–1520 cm^{-1} corresponding to the carbonyl group (C═O); and at 1240 cm^{-1} assigned to a single carbon-oxygen bond (C—O). All these groups belong to the ligands.

An intense and broad band located in the 3600–3100 cm^{-1} range is assigned to the O—H stretching vibration and confirms the existence of water due to the presence of absorbed moisture, which becomes more pronounced at the end of photolysis. No new bands that could be associated with the formation of an intermediate during photolysis of the precursors were apparent in the spectrum. This observation is consistent with the photo-induced loss of ligands from the precursor complexes, forming volatile products that are partially desorbed from the surface.

3.2. Characterization of the mixed-metal oxide thin films

FT-IR spectra for samples treated at different temperatures from 350

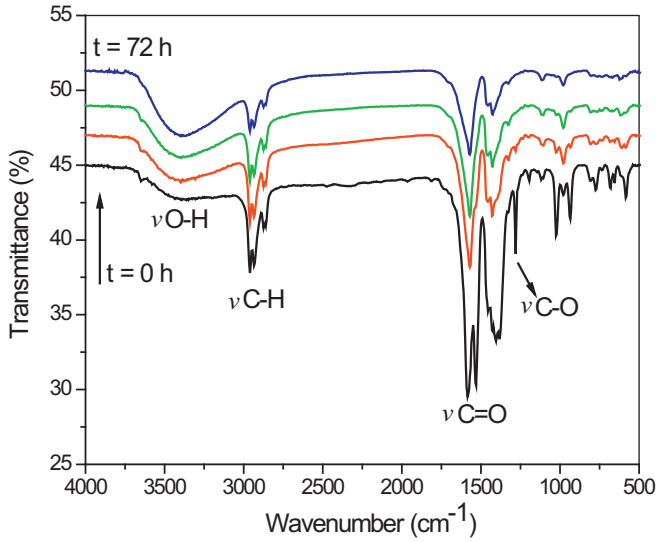

Fig. 1. FT-IR spectral changes associated with the photolysis of films of Ni(II) and Ga(III) complexes in a molar proportion of 1:2 and deposited on Si(100) for 0, 24, 48 and 72 continuous hours.

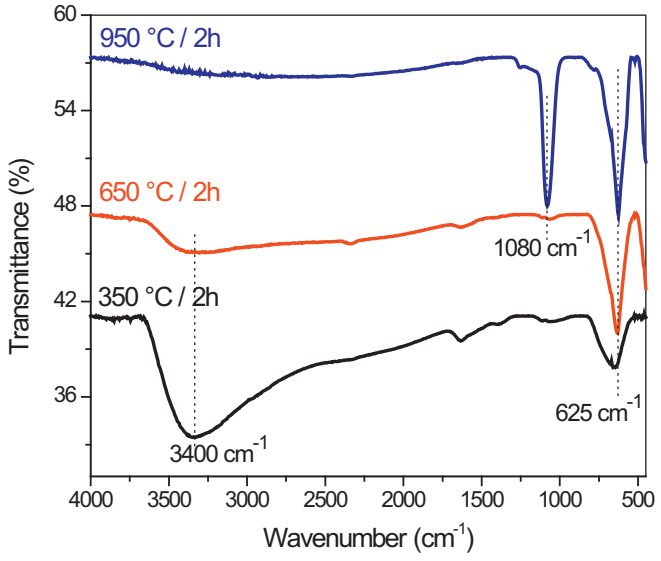

Fig. 2. FT-IR spectra for the photodeposited films of $NiGa_2O_4$ as a function of annealing temperature.

to 950 °C are shown in Fig. 2. For samples thermally treated at 350 and 650 °C, two hours was sufficient to remove organic residues, according to FT-IR spectroscopy, but insufficient for the formation of mixed-metal oxide thin films. Some authors [17] have reported that the peaks between 600 and 500 cm^{-1} and 500–400 cm^{-1} represent the characteristic metal-oxygen (A−O and B−O) vibrations, respectively, of the AB_2O_4 structure. It has also been reported [18] that the higher frequency bands (~750–550 cm^{-1}) can be attributed to metal-oxygen groups bond vibrations located in tetrahedral sites and that the lower frequency bands (~500–400 cm^{-1}) can be associated with the metal-oxygen bonding vibrations located at the octahedral sites. When the samples were annealed at 950 °C, it was possible to identify some characteristic peaks of the mixed-metal oxide films. The bands at 1080 and 625 cm^{-1} for the $NiGa_2O_4$ film can be attributed to Ni−O and Ga−O bond vibration modes, respectively. However, the broadening of both bands cannot confirm the formation of the regular spinel structure. The samples, exhibit a broad an intense band at ~3400 cm^{-1}, which can be assigned to the vibrational modes of O−H groups due to the absorption of traces of water molecules during the course of the measurement. With an increase in annealing temperature, the intensity of this signal decreases.

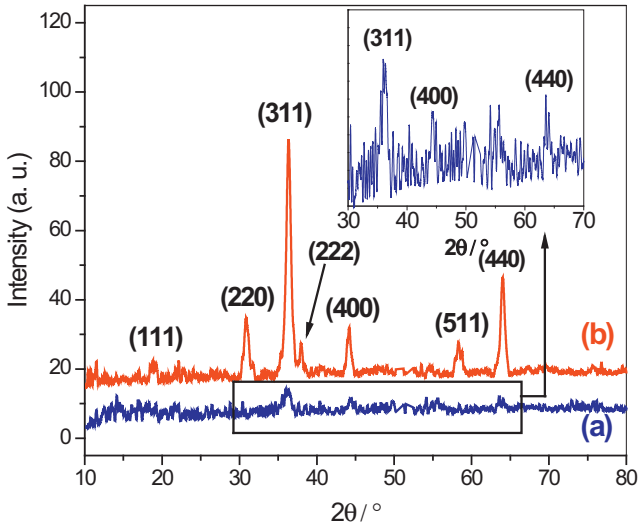

Fig. 3. XRD pattern of a photodeposited $NiGa_2O_4$:xEu film, where x = 15 mol% in the sample: (a) as-deposited and (b) annealed in air at 950 °C for 2 h.

Phase analysis and structural characterization of the samples were carried out by XRD studies. The XRD pattern (Fig. 3a) reveals the amorphous nature of the as-deposited films. Only peaks that can be attributed to the partial formation of spinel are observed. However, for films annealed at 950 °C (Fig. 3b), the XRD spectrum shows peaks at 2θ values of 63.8°, 58.1°, 43.8°, 37.7°, 36.0°, 30.6° and 18.6°, which correspond to the (440), (511), (400), (222), (311), (220) and (111) crystal planes of cubic $NiGa_2O_4$ with a spinel structure. Similar results have been reported in other articles [19–21]. No peaks attributable to other phases are observed, which indicates the formation of the pure phase of $NiGa_2O_4$. The introduction of europium as an additive in the crystalline structure of spinel does not modify their structure but can modify the lattice parameters due to the difference in the radius between the additive and the substituted ions in the spinel. We suggest that europium is not incorporated within the matrix by substituting for Ga^{3+} ions. It is known that the Eu^{3+} ion radius is 0.95 Å, which is slightly higher than the radius of Ga^{3+} (0.62 Å). Therefore, the incorporation of europium into the matrix occurs at the edges of each of the phases or the grain boundaries of the film. However, peaks ascribed to europium or its oxides states were not detected. It is possible that the content of europium in the matrix, are so low (at trace level), which is below the detection limit of XRD, or another possibility is that the species being well dispersed over the sample surface.

The chemical composition and surface electronic state of the samples annealed at 950 °C were analyzed by XPS. The survey XPS spectra are shown in Fig. 4, and they indicated the presence of Ni, Ga, O, and Eu in the $NiGa_2O_4$:xEu films.

The high resolution spectra of the Ga $2p_{3/2}$, O 1s and Ni $2p_{3/2}$ core levels were measured for the $NiGa_2O_4$:xEu sample and are shown in Fig. 5. The Ga $2p_{3/2}$ XPS (Fig. 5a) shows a main peak at approximately 1118.8 eV. This value is similar with those reported for Ga^{3+} in other spinels [6,22–24]. Fig. 5a (inset) shows the O 1s XPS spectra of the $NiGa_2O_4$:xEu sample. This spectrum presents two peaks, one located at 530.9 eV, associated with metal-oxygen bonds (M−O), and a second one at 532.5 eV, associated with the presence of hydroxyl species (O−H) on the surface, due to environmental moisture [6,25].

The interpretation of the XPS signal with respect to the formation of nickel oxides is widely debated. The Ni $2p_{3/2}$ spectra are often complex and contain multiple peaks, and therefore is difficult to assign specific binding energies to the different oxidation states of nickel. Some

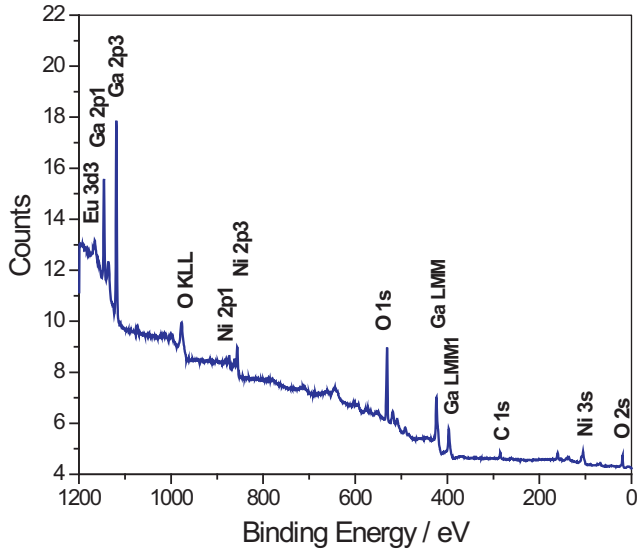

Fig. 4. XPS survey scan of the $NiGa_2O_4$:xEu films annealed at 950 °C for 2 h, where x = 15 mol% in the sample.

authors [26,27] have determined the position of Ni $2p_{3/2}$ binding energies at 852.6, 854.6 and 856.1 eV corresponding to Ni^0, Ni^{2+} and Ni^{3+} species, respectively. Moreover, each oxidation state is accompanied by major and minor peaks, as well as satellite peaks [28]. Other authors [29] associate the low energy Ni species at 854 eV to the Ni—O bonds of NiO, the peak centered at 856 eV to the formation of Ni—OH, while the peak centered around 857.8 eV is attributed to the formation of NiO(OH). The assignment of these Ni peaks to the formation of hydroxides is supported when the O 1s spectrum shows peaks in the range 531–532 eV range which to OH species.

In our case, the Ni $2p_{3/2}$ spectra (Fig. 5b) can be deconvoluted into four peaks, the main peak (1), the shoulder (2) and its satellites (3 and 4). The peak 1 at 856.2 eV as the main peak is ascribed to the chemical state Ni^{2+} or as NiO, and the peak 2 at 858.2 eV as the shoulder assigned to the Ni^{3+} or NiO(OH) species. The value obtained in the Ni $2p_{3/2}$ signal is similar with those reported for Nickel in other type of spinels [30,31].

The XPS spectra of Eu 3d for doped samples (not shown here) reveal two peaks, corresponding to Eu $3d_{5/2}$ at ~1136.0 eV and Eu $3d_{3/2}$ at ~1165.7 eV, with an energy separation (ΔE) of ~29.7 eV between the two peaks. These values are associated with the Eu^{3+} state [32,33]. No evidence for the existence of the Eu^{2+} state, such as satellite peaks associated with Eu $3d_{5/2}$ and Eu $3d_{3/2}$ signals, can be found [33,34].

The surface morphology of the samples was studied by scanning electron microscopy. Fig. 6a shows SEM images of the $NiGa_2O_4$:xEu samples, annealed at 950 °C. Here, it is possible to observe an irregular aspect with circular deposits corresponding to nucleation sites from the photo-reactivity and deposition of the precursor complexes.

Fig. 6b shows EDX spectrum and the percentages of each element obtained from EDX analysis are presented in Table 1. The SEM-EDX results confirm the existence of each of the elements (Ni, Ga and Eu) but in a low percentage. The high carbon content is attributable to organic byproducts of the photolysis of the precursor complexes, whereas the high oxygen content is probably due to the oxidation of each of the elements, as well as oxidation of the substrate due to surface annealing.

3.3. Optical properties

The optical properties of the Eu-doped $NiGa_2O_4$ were examined using a UV–vis spectrophotometer. Fig. 7 shows the optical transmission spectra of the photodeposited samples on fused quartz that were annealed at 950 °C and had a ~200 nm thickness. It can be seen from

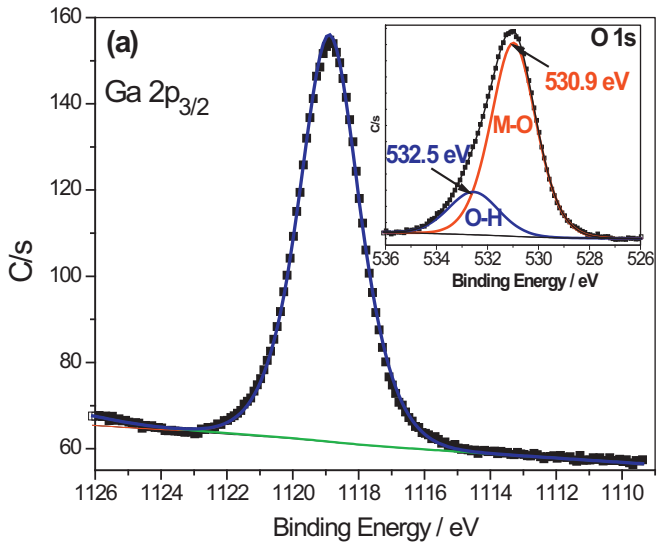

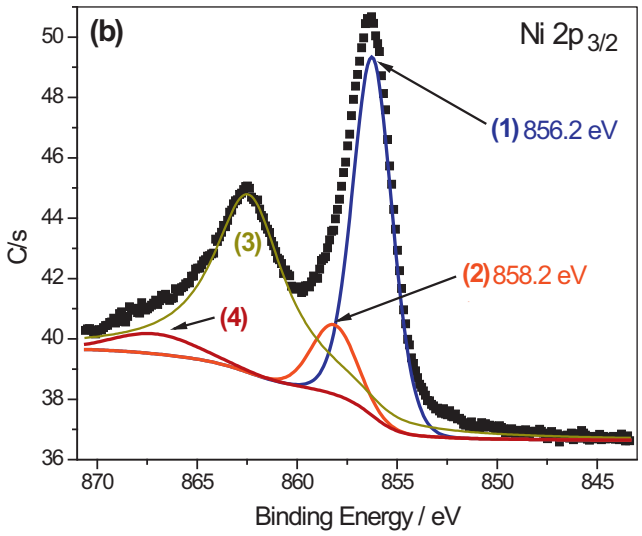

Fig. 5. High-resolution XPS spectra of the $NiGa_2O_4$:xEu sample annealed in air at 950 °C for 2 h: (a) Ga $2p_{3/2}$ spectrum (inset: O 1s spectra) and (b) Ni $2p_{3/2}$ spectrum.

the UV–vis spectra that the transmittance of the films is > 85% in the visible range for all samples. There is also a slight absorption at 250 nm which can be attributed to $NiGa_2O_4$ host lattice [35,36]; however, with the increase of europium doping concentration, it is possible to observe a gradual increase in the absorption due charge transfer absorption from oxygen to europium [37].

The slight decrease in transmittance in the doped samples can be attributed to the greater thickness due to a higher concentration of dopant. The optical band gap of the samples was determined by applying the absorption coefficient α, calculated using the previous measured transmittance data, from the relation:

$$\alpha = \frac{1}{t}\ln\left(\frac{1}{T}\right) \quad (2)$$

where t is the thickness of the thin film and T is the transmittance of the sample. For a crystalline semiconductor, it has been shown that the optical absorption near the band edge follows the equation:

$$(\alpha h\nu)^n = B(h\nu - E_g) \quad (3)$$

where B is a constant, E_g is the band gap energy, α is the absorption coefficient and h is Planck's constant. Among the parameters, n determines the transition characteristics of a semiconductor. The band

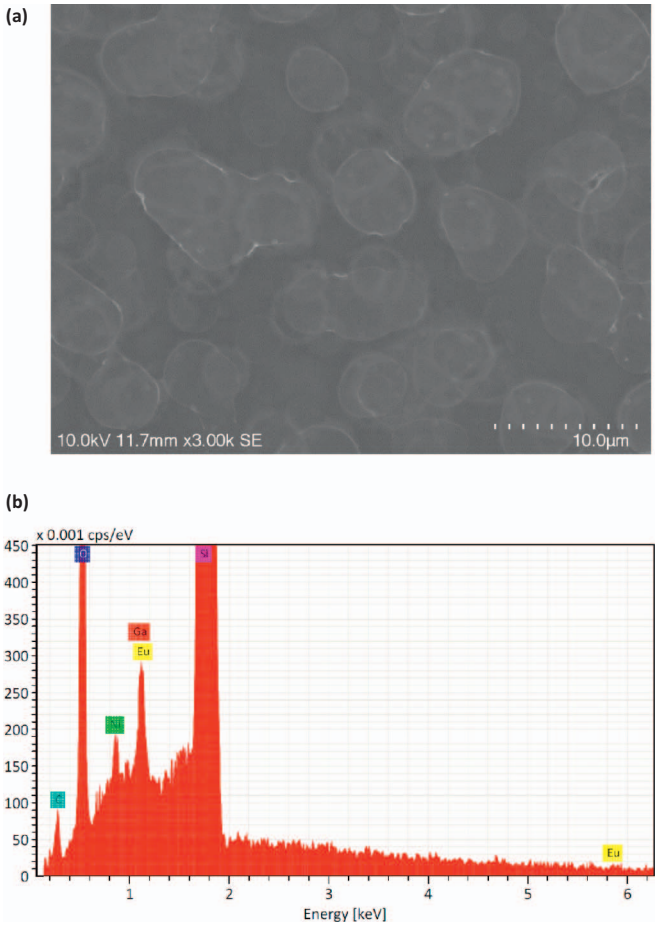

Fig. 6. (a) SEM image of the $NiGa_2O_4$:xEu sample annealed at 950 °C for 2 h. (b) the corresponding EDX spectrum. With x = 15 mol% europium.

Table 1
Percentage of each element obtained from SEM-EDX analysis of the sample annealed at 950 °C.

Sample/element	O-K atom (%)	Ni-L atom (%)	Ga-L atom (%)	Eu atom (%)	C-K atom (%)	Ni/Ga
$NiGa_2O_4$:xEu	69.95	0.58	1.20	0.13	28.14	0.48

gap energy can be estimated by plotting $(\alpha h\nu)^2$ as a function of photon energy ($h\nu$) and extrapolating the linear portion of the curve to the point where the absorption coefficient (α) equals zero, and this value is presented in Fig. 7. The calculated values of the optical band gaps of the undoped $NiGa_2O_4$ films were 4.75 eV. The band gap of the Eu-doped samples are slightly lower than those of the undoped samples, this phenomenon can be explained; due to introduction of additives and the presence of oxygen vacancies in the material provide discrete energy levels in the energy gap between the conduction and valence bands of the host material. The calculated values for the band gap of the $NiGa_2O_4$ samples are higher than those reported in other studies, 3.85 eV [38] and 3.53 eV [39].

This variation in the values of band gap to higher energy, which was observed in other transition metal oxides [40], is due to the existence of morphological imperfections of the film, as well as to the presence of grain boundaries. These characteristics lead to larger free carrier concentrations and the existence of potential barriers. The electric fields arising from these factors in the disordered state result in an increase in the optical band gap [40,41]. In this case, the heterogeneity and the presence of imperfections observed by SEM in our films are probably

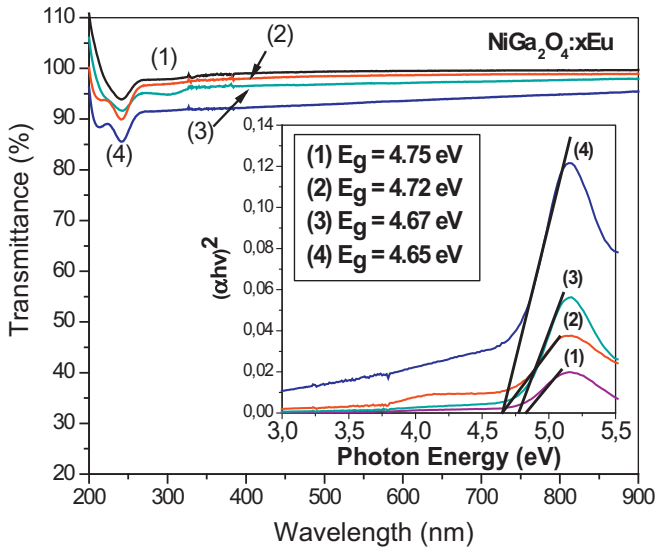

Fig. 7. Transmittance spectra for $NiGa_2O_4$:xEu thin films. The inset shows the estimation of the optical band gap energy, E_g, of the samples, with (1) x = 0, (2) x = 5, (3) x = 10 and (4) x = 15 mol% Eu.

the cause for the obtained wide band gap values.

3.4. Luminescent characteristics

The excitation and emission spectra of the $NiGa_2O_4$:xEu films annealed at 950 °C are illustrated in Fig. 8. The excitation spectrum (Fig. 8a) obtained by monitoring the emission of Eu(III) $^5D_0 \rightarrow {}^7F_2$ luminescence at 610 nm mainly consists of a broad intense band with a maximum at 266 nm and a series of broad bands in the 255–370 nm range, which are assigned to f-f transitions of europium ions. The band at 266 nm is assigned to the charge transfer of electrons from the 2p orbital of oxygen to the 4f orbital of europium, together with the absorption of the $NiGa_2O_4$ host lattice. The charge transfer band increases with europium concentration, but it decays when the europium concentration reaches 15 mol%. The emission spectrum (Fig. 8b) obtained by excitation at 325 nm shows characteristic emission peaks of Eu^{3+} between 500 and 750 nm, which are associated with the following transitions: $^5D_0 \rightarrow {}^7F_0$ at 573 nm, $^5D_0 \rightarrow {}^7F_1$ at 595 nm, $^5D_0 \rightarrow {}^7F_2$ at 610 nm, $^5D_0 \rightarrow {}^7F_3$ at 658 nm and $^5D_0 \rightarrow {}^7F_4$ at 700 nm. Similar results have been reported with Eu^{3+} incorporated in other spinel-type structures [6,42]. However, we can see that the emission signal of the europium are presented in the form of broad band very different from the sharp signals of emission of the europium when it is inserted in a crystalline material.

Some authors [43] argue that this feature is an indication that europium may be located at the surface or close to surface sites, instead of entering the crystal lattice of the host material. It is known that the Eu^{3+} ion radius is 0.95 Å, which is larger than the radius of Ga^{3+} (0.62 Å). Therefore, the probability of Eu^{3+} ions entering the lattice of $NiGa_2O_4$ by substituting for Ga^{3+} is very low. Most likely, the Eu^{3+} ions penetrate into the amorphous regions at the grain boundaries of the films, considering that the emission spectrum obtained is similar to that of Eu^{3+} in other amorphous hosts [6]. In other words, the presence of structural defects in the material can potentially cause the Eu^{3+} ions to experience various crystal field environments, and therefore the photoluminescence spectrum will be broadened inhomogeneously [44].

When a lanthanide ion (Ln^{III}) is incorporated into a host material, the energy level of the Ln^{III} ion is generally split into a number of sublevels due to the crystal field. These sublevels can generate emission signals different from what one can expect from the emission bands of a crystalline material doped because due to multiple of f-f transitions of the Ln^{III} ion. These electronic transitions respond to the relation 2j + 1

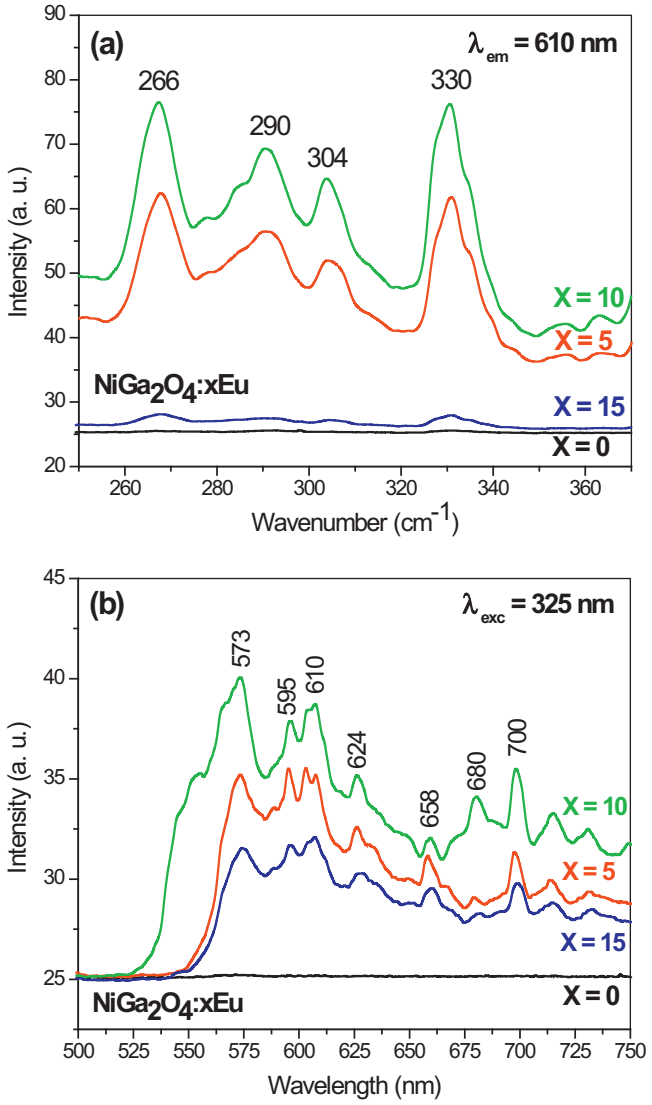

Fig. 8. Photoluminescence (a) excitation and (b) emission spectra of $NiGa_2O_4$:xEu annealed at 950 °C, where x = 0, 5, 10 and 15 mol% Eu.

(where j is the electronic angular momentum) [45]. Therefore, there should be only one peak for the $^7F_{J=0}$ level, at least three peaks for the $^7F_{J=1}$ level, and at least five peaks for the $^7F_{J=2}$ level. However, it is also well known that the maximum number of these sublevels depends on the symmetry of the crystal field surrounding the Ln^{III} ion [45]. Hence, other signals are seen here that are different than those mentioned previously: one at 624 nm and another located at 680 nm, attributed to $^5D_0 \rightarrow {}^7F_2$ and $^5D_0 \rightarrow {}^7F_3$ transitions, respectively. It has been reported [45] that the observation of other peaks produced by the splitting of ^7F_j levels are the result of dopant Ln^{III} ions randomly occupying different sites in the host material.

Based on the above results and discussion, a schematic diagram is illustrated to explain the luminescent characteristics of the mixed oxide samples (Fig. 9). The incorporation of additives (Eu ions) into the $NiGa_2O_4$ lattice, provides discrete energy levels in the energy gap between the conduction and valence bands in the host material called defect states. These defect sates can be sources of electrons and also sites of capture of excited electrons under ultraviolet light irradiation. Here, the absorption of light at 325 nm (3.8 eV) produces the generation of a number of holes and electrons. Subsequently, photoexcited electrons in the defect states may migrate to different excited states of Eu^{3+} ion (in this case, only the $^5D_0$ level is shown) through the process of energy transfer (ET). Finally, excited photoelectrons at the excited levels of Eu^{3+} can radiatively relax from $^5D_0$ to various ^7F_j (j = 0–4) ground levels of Eu^{3+}, resulting in emission in the visible region (570–700 nm).

In this way, energy transfer from $NiGa_2O_4$ to Eu^{3+} ions can be facilitated through energy trapping centers in the host material. These energy capture centers are a product of the intrinsic or extrinsic defects of host material. In other words, the structure of the material, the type of additive incorporated and the discrete energy levels between the host material and the additive are determinant in the energy transfer process [46].

4. Conclusions

In summary, nickel gallium oxide spinels were prepared by a solid-state photochemical method, followed by post-annealing at 950 °C. The results of XRD and XPS analyses show spinel formation in the $NiGa_2O_4$ samples. When these films are doped with different concentrations of Eu(III) and excited at 325 nm, they exhibit emission corresponding to $^5D_0 \rightarrow {}^7F_j$ (j = 0–4) transitions of Eu(III) ions. The photoluminescence

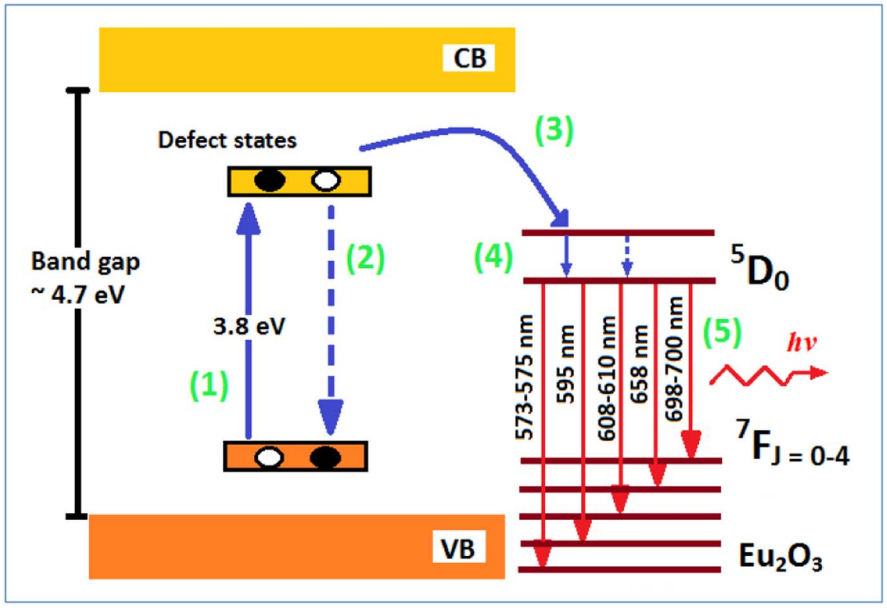

Fig. 9. Schematic of the energy transfer mechanism from the host material to Eu^{3+}: (1) excitation process by absorption of light at 325 nm, (2) non-radiative transitions between defect states of the host material (recombination process), (3) energy transfer process from defect states to the excited level of Eu^{3+}, (4) non-radiative transitions from excited levels to the $^5D_0$ level of Eu^{3+} and, (5) radiative transitions from the $^5D_0$ level to the ^7F_j (j = 0, 1, 2, 3 and 4) ground levels of Eu^{3+}.

spectra show broad and irregular bands probably due to the existence of structural defects caused by a very irregular deposition of the material, which imparts imperfections in its morphology, regardless of the chemical composition of the film. The presence of these defects suggests a possible energy transfer from the matrix to the europium ions, which produces the emission processes. Further studies are necessary to better control the morphology and structure in the photochemical synthesis of spinels in order to improve the optical properties of the material. The use of a single-source precursor species with metal ratios compatible to targeted ceramic material may contribute to better control in the deposition of the material as has been proposed in other synthetic methodologies [47,48].

Acknowledgments

The authors are grateful to FONDECYT (National Fund for Scientific and Technological Development), Chile, Grant No 1130114, for financial support and to CONICYT-FONDEQUIP Program (No EQM-140088) for the acquisition of Hitachi Scanning Electron Microscope (SEM). We are grateful to the post-graduate office at University of Bío-Bío (Plan Plurianual 2016–2020).

References

[1] G. Cabello, L. Lillo, C. Caro, M. Seguel, C. Sandoval, G.E. Buono-Core, B. Chornik, M. Flores, A photochemical proposal for the preparation of $ZnAl_2O_4$ and $MgAl_2O_4$ thin films from β-diketonate complex precursors, Mater. Res. Bull. 77 (2016) 212–220.
[2] J. Shi, W. Yu, I. Bergmann, H. Bremers, V. Sepelak, W. Mader, K.D. Becker, Synthesis and characterization of nonstoichiometric $NiGa_2O_4$ transparent thin films, J. Alloys Compd. 504S (2010) S432–S434.
[3] J.D.S. Walker, J.R. Hayes, A.P. Grosvenor, Examination of the site preference of metals in $NiAl_{2-x}Ga_xO_4$ spinel-type oxides by X-ray absorption near-edge spectroscopy, J. Electron Spectrosc. Relat. Phenom. 195 (2014) 139–144.
[4] B. Szpikowska-Sroka, N. Pawlik, T. Goryczka, W.A. Pisarski, Technological aspects for Tb^{3+}-doped luminescent sol–gel nanomaterials, Ceram. Int. 41 (2015) 11670–11679.
[5] R.J. Wiglusz, T. Grzyb, A. Watras, P.J. Deren, S. Lis, W. Strek, An impact of sintering temperature and doping level on structural and spectral properties of Eu-doped strontium aluminium oxide, J. Rare Earths 29 (2011) 1105–1110.
[6] X. Duan, F. Yu, Y. Wu, Synthesis and luminescence properties of $ZnGa_2O_4$ spinel doped with Co^{2+} and Eu^{3+} ions, Appl. Surf. Sci. 261 (2012) 830–834.
[7] Hai Liu, Lixin Yu, Fuhai Li, Photoluminescent properties of Eu^{3+} and Dy^{3+} ions doped $MgGa_2O_4$ phosphors, J. Phys. Chem. Solids 74 (2013) 196–199.
[8] Xinsheng Liu, Chapter 6: inorganic photochemical synthesis, in: Ruren Xu, Wenqin Pang, Qisheng Huo (Eds.), Modern Inorganic Synthetic Chemistry, Elsevier, 2011, pp. 129–150.
[9] G. Cabello, L. Lillo, C. Caro, M. Seguel, G.E. Buono-Core, Y. Huentupil, B. Chornik, C. Carrasco, C.A. Rodríguez, Synthesis, characterization and optical properties of $ATiO_3$–Pr thin films prepared by a photochemical method (where A = Ba and Ca), Mater. Res. Bull. 70 (2015) 32–39.
[10] G. Cabello, A. Araneda, L. Lillo, C. Caro, C. Venegas, M. Tejos, B. Chornik, Application of photochemical method in the synthesis of Ga_2O_{3-x} thin films co-doped with terbium and europium, Solid State Sci. 27 (2014) 24–29.
[11] G. Cabello, L. Lillo, C. Caro, M.A. Soto-Arriaza, B. Chornik, G.E. Buono-Core, Evaluation on the optical properties of Ga_2O_{3-x} thin films co-doped with Tb^{3+} and transition metals (Mn^{2+}, Cr^{3+}) prepared by a photochemical route, Ceram. Int. 39 (2013) 2443–2450.
[12] S. Giuffrida, G.G. Condorelli, L.L. Costanzo, G. Ventimiglia, R. Lo Nigro, M. Favazza, E. Votrico, C. Bongiorno, I.L. Fragala, Nickel nanostructured materials from liquid phase photodeposition, J. Nanopart. Res. 9 (2007) 611–619.
[13] J.L. Rodriguez, M.A. Valenzuela, H. Tiznado, T. Poznyak, E. Flores, Synthesis of nickel oxide nanoparticles supported on SiO_2 by sensitized liquid phase photodeposition for applications in catalytic ozonation, J. Mol. Catal. A Chem. 392 (2014) 39–49.
[14] G.E. Buono-Core, M. Tejos, R. Schrebler, A.H. Klahn, R.H. Hill, Nickel tropolonate complexes as precursors for the direct photodeposition of NiO thin films, J. Chil. Chem. Soc. 49 (3) (2004) 223–226.
[15] W.C.H. Chu, S.L. Blair, R.H. Hill, Photochemistry of bis-triphenylphosphine nickel dicarbonyl on silicon surfaces: the lithographic deposition of nickel and nickel-iron, nickel-chromium and iron-chromium containing films, J. Mater. Sci. 37 (2002) 3685–3691.
[16] G. Cabello, L. Lillo, Y. Huentupil, F. Cabrera, G.E. Buono-Core, B. Chornik, A simple photochemical method to synthesize Ga_2O_3–Dy^{3+}–M^{3+} thin films and their evaluation as optical materials (where M = Cr or Co), J. Phys. Chem. Solids 72 (2011) 1170–1174.
[17] M. Yu, J. Lin, Y.H. Zhou, S.B. Wang, Citrate–gel synthesis and luminescent properties of $ZnGa_2O_4$ doped with Mn^{2+} and Eu^{3+}, Mater. Lett. 56 (2002) 1007–1013.
[18] V.R. Kumar, K.V. Narasimhulu, N.O. Gopal, R.P.S. Ha-Kyun Jung, J. Chakradhar, Lakshmana Rao, EPR, luminescence and IR studies of Mn activated $ZnGa_2O_4$ phosphor, J. Phys. Chem. Solids 65 (2004) 1367–1372.
[19] H. Xue, Z. Li, Z. Ding, L. Wu, X. Wang, X. Fu, Hollow rods of nanocrystalline $NiGa_2O_4$: hydrothermal synthesis, formation mechanism, and application in photocatalysis, Cryst. Growth Des. 12 (2008) 4511–4516.
[20] M. Kerlau, O. Merdrignac-Conanec, P. Reichel, N. Barsan, U. Weimar, Preparation and characterization of gallium (oxy)nitride powders. Preliminary investigation as new gas sensor materials, Sensors Actuators B Chem. 115 (2006) 4–11.
[21] L. Chen, T. Horiuchi, T. Mori, Catalytic reduction of NO over a mechanical mixture of $NiGa_2O_4$ spinel with manganese oxide: influence of catalyst preparation method, Appl. Catal., A 209 (2001) 97–105.
[22] S. Wu, J. Xue, R. Wang, J. Li, Synthesis, characterization and microwave dielectric properties of spinel $MgGa_2O_4$ ceramic material, J. Alloys Compd. 585 (2014) 542–548.
[23] J. Liu, X. Duan, N. Li, H. Jiang, Effects of synthesis method on cation distribution and optical properties of Co/Cr co-doped $MgGa_2O_4$ nanoparticles, J. Alloys Compd. 640 (2015) 169–174.
[24] X. Duan, J. Liu, X. Wang, H. Jiang, Cation distribution and optical properties of Cr-doped $MgGa_2O_4$ nanocrystals, Opt. Mater. 37 (2014) 851–854.
[25] J.C. Dupin, D. Gonbeau, P. Vinatier, A. Levasseur, Systematic XPS studies of metal oxides, hydroxides and peroxides, Phys. Chem. Chem. Phys. 2 (2000) 1319–1324.
[26] K.S. Usha, R. Sivakumar, C. Sanjeeviraja, Vasant Sathe, V. Ganesan, T.Y. Wange, Improved electrochromic performance of a radio frequency magnetron sputtered NiO thin film with high optical switching speed, RSC Adv. 6 (2016) 79668–79680.
[27] B. Polteau, F. Tessier, F. Chevire, L. Cario, F. Odobel, S. Jobic, Synthesis of Ni-poor NiO nanoparticles for p-DSSC applications, Solid State Sci. 54 (2016) 37–42.
[28] K. Sajilal, A. Moses Ezhil Raj, Effect of thickness on structural and magnetic properties of NiO thin films prepared by chemical spray pyrolysis (CSP) technique, Mater. Lett. 164 (2016) 547–550.
[29] A. Villa, G.M. Veith, D. Ferri, A. Weidenkaff, K.A. Perry, S. Campisia, L. Prati, NiO as a peculiar support for metal nanoparticles in polyols oxidation, Catal. Sci. Technol. 3 (2013) 394–399.
[30] A. Horváth, L. Guczi, A. Kocsonya, G. Sáfrán, V. La Parola, L.F. Liotta, G. Pantaleo, A.M. Venezia, Sol-derived $AuNi/MgAl_2O_4$ catalysts: formation, structure and activity in dry reforming of methane, Appl. Catal., A 468 (2013) 250–259.
[31] Anne Ponchel, Alain DĬHuysser, Carole Lamonier, Louise Jalowiecki-Duhamel, $CeNi_xO_y$ and $CeAl_zNi_xO_y$ solids studied by electron microscopy, XRD, XPS and depth sputtering techniques, Phys. Chem. Chem. Phys. 2 (2000) 303–312.
[32] G. Sheng, H. Dong, R. Shen, Y. Li, Microscopic insights into the temperature-dependent adsorption of Eu (III) onto titanate nanotubes studied by FTIR, XPS, XAFS and batch technique, Chem. Eng. J. 217 (2013) 486–494.
[33] S. Kumar, R. Prakash, R.J. Choudhary, D.M. Phase, Structural, XPS and magnetic studies of pulsed laser deposited Fe doped Eu_2O_3 thin film, Mater. Res. Bull. 70 (2015) 392–396.
[34] M.Y.A. Yagoub, H.C. Swart, L.L. Noto, J.H. O'Connel, M.E. Lee, E. Coetsee, The effects of Eu-concentrations on the luminescent properties of SrF_2: Eu nanophosphor, J. Lumin. 156 (2014) 150–156.
[35] L.L. Noto, D. Poelman, V.R. Orante-Barrón, H.C. Swart, L.E. Mathevula, R. Nyenge, M. Chithambo, B.M. Mothudi, M.S. Dhlamini, Photoluminescence and thermoluminescence properties of $BaGa_2O_4$, Phys. B (2017), http://dx.doi.org/10.1016/j.physb.2017.07.059.
[36] L.L. Noto, S.K.K. Shaat, D. Poelman, M.S. Dhlamini, B.M. Mothudi, H.C. Swart, Cathodoluminescence mapping and thermoluminescence of Pr^{3+} doped in a $CaTiO_3/CaGa_2O_4$ composite phosphor, Ceram. Int. 42 (2016) 9779–9784.
[37] N. Lakshminarasimhan, U.V. Varadaraju, Role of crystallite size on the photoluminescence properties of $SrIn_2O_4$:Eu^{3+} phosphor synthesized by different methods, J. Solid State Chem. 181 (2008) 2418–2423.
[38] S.X. Zhou, X.J. Lu, C. Zhang, X. Huang, L. Kang, Z.S. Lin, Y. Chen, W.F. Fu, Synthesis of $NiGa_2O_4$ octahedron nanocrystal with exposed {111} facets and enhanced efficiency of photocatalytic water splitting, ChemPlusChem 80 (2015) 223–230.
[39] X.J. Lu, S. Zhou, X. Huang, C. Wang, W.F. Fu, Photocatalytic overall water splitting promoted by SnOx–$NiGa_2O_4$ photocatalysts, Appl. Catal. B Environ. 182 (2016) 220–228.
[40] C.V. Ramana, R.J. Smith, O.M. Hussain, C.C. Chusuei, C.M. Julien, Correlation between growth conditions, microstructure, and optical properties in pulsed-laser-deposited V_2O_5 thin films, Chem. Mater. 17 (2005) 1213–1219.
[41] M.F. Malek, M.H. Mamat, M.Z. Musa, T. Soga, S.A. Rahman, Salman A.H. Alrokayan, Haseeb A. Khan, M. Rusop, Metamorphosis of strain/stress on optical band gap energy of ZAO thin films via manipulation of thermal annealing process, J. Lumin. 160 (2015) 165–175.
[42] M. Vasile, P. Vlazan, N.M. Avram, Characterization and optical properties of $ZnGa_2O_4$:Eu^{3+} nanophosphor grown by hydrothermal method, J. Alloys Compd. 500 (2010) 185–189.
[43] C. Peng, G. Li, D. Geng, M. Shang, Z. Hou, J. Lin, Fabrication and luminescence properties of one-dimensional $ZnAl_2O_4$ and $ZnAl_2O_4$: A^{3+} (A = Cr, Eu, Tb) microfibers by electrospinning method, Mater. Res. Bull. 47 (2012) 3592–3599.
[44] H. Zhu, R. Li, W. Luo, X. Chen, Eu^{3+}-doped β-Ga_2O_3 nanophosphors: annealing effect, electronic structure and optical spectroscopy, Phys. Chem. Chem. Phys. 13 (2011) 4411–4419.
[45] Y. Kang, B. Thuy, Y. Shimokawa, T. Hayakawa, S. Sakaida, L. Miao, S. Tanemura, S. Honda, Y. Iwamoto, Relationship between Eu^{3+} substitution sites and photoluminescence properties of $SrIn_2O_4$:Eu^{3+} spinel phosphors, J. Lumin. 169 (2016) 78–85.
[46] S.M. Ahmed, P. Szymanski, M.A. El-Sayed, Y. Badr, L.M. El-Nadi, The photoluminescence properties of undoped and Eu-doped ZnO thin films grown by RF sputtering on sapphire and silicon substrates, Appl. Surf. Sci. 359 (2015) 356–363.
[47] F. Meyer, R. Hempelmann, S. Mathur, M. Veith, Microemulsion mediated sol–gel synthesis of nano-scaled MAl_2O_4 (M = Co, Ni, Cu) spinels from single-source heterobimetallic alkoxide precursors, J. Mater. Chem. 9 (1999) 1755–1763.
[48] S. Mathur, S. Barth, H. Shen, Chemical vapor growth of $NiGa_2O_4$ films: advantages and limitations of a single molecular source, Chem. Vap. Depos. 1 (2005) 11–16.